Chemical synthesis of hollow sea urchin like nanostructured polypyrrole particles through a core-shell redox mechanism using a MnO2 powder as oxidizing agent and sacrificial nanostructured template

Lynda Benhaddad, Marie-Claude Bernard, Claude Deslouis, Laid Makhloufi, Bouzid Messaoudi, Alain Pailleret, Hisasi Takenouti

Chemical synthesis of hollow sea urchin like nanostructured polypyrrole particles through a core-shell redox mechanism using a MnO_2 powder as oxidizing agent and sacrificial nanostructured template

L. Benhaddad [a,b,c], M.C. Bernard [b,c], C. Deslouis [b,c], L. Makhloufi [a], B. Messaoudi [a], A. Pailleret [b,c,*], H. Takenouti [b,c]

Corresponding author:
E-mail:alain.pailleret@upmc.fr; Tel: +33 1 44 27 41 69; Fax: +33 1 44 27 40 74

[a]*Laboratoire de Technologie des Matériaux et Génie des Procédés (LTMGP). Département de Génie des Procédés. Université A. Mira, Route de Targa Ouzemmour, 06000 Béjaia, Algeria.*

[b]*CNRS, UPR 15, Laboratoire Interfaces et Systèmes Electrochimiques, (LISE, case courrier 133), 4 Place Jussieu, F-75005, Paris, France*

[c]*UPMC Univ. Paris VI, UPR 15, LISE, 4 Place Jussieu, F-75005, Paris, France*

Abstract

Hollow sea urchin shaped nanostructured polypyrrole powder was successfully synthesized chemically in an acidic medium through a core-shell redox mechanism by using a nanostructured MnO_2 powder as oxidizing agent and sacrificial template simultaneously. The morphology and the structure of MnO_2 powder based reactant and produced polypyrrole powder were characterized respectively by using FEG-SEM, TEM, EDX and XRD techniques, which led us to demonstrate clearly the formation of hollow and open microparticles of polypyrrole with the presence of nanotubes on their surface. Nanostructured polypyrrole powder was found to be rather amorphous even though the shape of the polypyrrole particles was induced by the crystalline and nanostructured sea urchin shaped MnO_2 powder on which they grew. In addition, neither MnO_2 nor any manganese based species were found within the produced polypyrrole powder, which ruled out the production of composite materials. Moreover, Raman technique showed that the synthesized PPy powder

was produced in the oxidized and thus conducting state. It actually possesses a 0.31 doping level and a 0.05 $S.cm^{-1}$ conductivity, as shown by XPS and impedance spectroscopy measurements respectively. Cyclic voltammetry and UV-Visible spectroscopy studies allowed us to identify the oxidation mechanism of pyrrole by our MnO_2 powder through the detection of soluble Mn^{2+} cations as reaction products isolated after filtration of the reaction medium.

Keywords: polypyrrole powder; nanostructuration; core-shell redox mechanism; manganese dioxide; sacrificial template; reactive template.

1. Introduction

The term “nanomaterials” encompasses a wide range of materials including nanocrystalline materials, nanocomposites, nanoparticles, and nanotubes for example. Recently, the synthesis of nanomaterials has attracted a great scientific interest due to their unique physical, chemical, electrical, and magnetic properties, resulting mostly from their small size and their high specific area [1-5], which makes them eligible for a vast range of application domains.

In particular, conducting polymers have been intensively studied for their one-dimensional conjugated structures as well as their adjustable conductivity and surface reactivity [6–9]. Furthermore, nanostructured conducting polymers such as nanoparticles [10, 11], nanofibres [12, 13], nanotubes [14] and nanowires [15-17] have received great attention, mainly for their promising applications in batteries, conducting paints, chemical and electrochemical sensors, and field emission applications [7,18–20]. Polypyrrole (PPy) is one of the most investigated conducting polymers as a consequence of its high electrical conductivity, relatively good stability in air, low toxicity and simple preparation [7, 8, 21–24]. Generally, two methods can be used to prepare polypyrrole, namely electrochemical and chemical polymerizations. Both

can involve a template during the polymerisation of pyrrole so as to obtain polypyrrole nanostructures [25, 26].

Template synthesis is an elegant approach for the elaboration of nanostructures. For example, it may involve the synthesis of a desired material within the pores of a nanoporous membrane [27]. In fact, two types of templates have been reported in literature: hard templates such as porous polycarbonate films [28], fibrillar V_2O_5 [29], and porous alumina [30], which usually have to be removed after synthesis of nanostructured polypyrrole, with the risk to destroy the synthesized polypyrrole, or some of its main properties, due to the use of strongly acidic/basic aqueous or organic solutions or elevated temperatures [25], and soft templates such as reverse microemulsions [31] and micelles [32], that may have the disadvantages of instability, low efficiency and lack of versatility for a given monomer [25].

Among targeted structured materials, hollow spheres have received enormous interest in recent years due to their unique properties and their numerous potential applications in various domains as delivery vehicles for the removal of contaminated waste and the controlled release of substances such as drugs, cosmetics, dyes and inks or as a catalyst carrier [33]. In order to improve the processability of polypyrrole, great efforts have been made to prepare polypyrrole hollow spheres. Recently, polymeric hollow spheres have been cited as novel types of carriers and nanoreactors with designed properties because they exhibit controllable permeability and surface functionality, which should enable many applications [34-37]. As a result, many efforts are made up to now to find out a facile, efficient and versatile approach to synthesize nanostructured polypyrrole based materials but it remains a key research challenge for researchers.

To this end, we introduce in this contribution a simple and efficient chemical method to synthesize pure nanostructured polypyrrole powder from an acidic aqueous medium by using

nanostructured manganese dioxide. MnO_2 was already mentioned in literature as a possible oxidizing agent to produce conducting polymers from corresponding soluble monomers. It was indeed observed for instance by N. Ballav *et al.* that MnO_2, PbO_2, and NH_4VO_3 particles can act as oxidants for the polymerization of aniline to produce polyaniline without acting as templates [38]. These oxidizing species are recoverable and recyclable, which is an advantage over conventional oxidizing agent $(NH_4)_2S_2O_8$ [38]. The chemical synthesis of pure nanostructured polyaniline powders from an adequate solution by using MnO_2 powder as an oxidizing agent and a template simultaneously was also reported [39]. However, if the experimental conditions are not adequate, then a PANI/MnO_2 composite material is formed [40-42]. We also noticed from literature that MnO_2 was claimed to act as an oxidizing agent towards the pyrrole monomer to produce PPy/MnO_2 composite materials [43-44]. Nevertheless, to the best of our knowledge, literature does not contain any report of the exact and accurate mechanism (stoechiometry, other reaction products except PPy, properties of PPy) of the chemical synthesis of polypyrrole powders using a MnO_2 powder.

The objective of the present study was thus aimed at defining the mechanism of the chemical polymerization of pyrrole into nanostructured polypyrrole materials from an acidic medium with the help of a MnO_2 powder synthesized by a hydrothermal method and used as oxidizing agents and sacrificial nanostructured template simultaneously.

The structures and morphologies of all powders synthesized in this work were characterized by various methods: Field Emission Gun-Scanning Electron Microscope (FEG-SEM), Transmission Electron Microscopy (TEM), Energy Dispersive X-ray elemental analysis (EDX), and X-ray Diffraction (XRD) techniques and Raman spectroscopy. UV-Visible spectroscopy was used in the presence of a binding agent that is specific for the detection of Mn^{2+} cations, as well as cyclic voltammetry. Our purpose was to accurately and undoubtedly

identify the manganese based reaction product of the formation mechanism of our nanostructured polypyrrole powders in the filtrated reaction medium.

2. Experimental Section

2.1. Chemicals

All the solutions were prepared using water deionised with double ion exchange columns. Manganese sulphate ($MnSO_4$, H_2O), sulphuric acid (H_2SO_4), and sodium persulphate ($Na_2S_2O_8$) were purchased from Prolabo. The latter compound was used as oxidizing agent towards Mn^{2+} cations for the synthesis of MnO_2 powder. Pyrrole was purchased from Fluka (97 % purity) and was purified by distillation. 25,26,27,28-tetrahydroxy-calix[4]arene-5,11,17,23-tetrasulfonic acid ($C_{28}H_{24}O_{16}S_4$), noted Calix-S_4, and sodium hydroxide (NaOH) were purchased from Acros Organics and Prolabo respectively and used as received.

2.2. Synthesis of powders

MnO_2: This method has already been reported in our previous publications [4,5]. It consists in mixing $MnSO_4$, H_2O (0.08 mol) with $Na_2S_2O_8$ (0.08 mol) and 150 mL of deionised water at room temperature. The mixture was stirred during 10 min so as to form a homogeneous pink solution that was then kept at 90 °C for 24 h. The obtained powder was filtered, rinsed with deionised water several times, and finally dried at 60 °C for 24 h.

Polypyrrole: The polypyrrole powders were chemically prepared by injecting liquid pyrrole ($V_{pyrrole}$ = 1.36 mL, 0.2 M) into a beaker containing MnO_2 powder (2 g) suspended in an aqueous solution of sulphuric acid (100 mL, 1 M) at room temperature. The polymerization of pyrrole was found to be initiated immediately after addition of the monomer to the medium. The mixture was stirred magnetically for 4 hours at room temperature. The black precipitate

of polypyrrole was collected by filtration, rinsed repeatedly with deionised water, and finally dried at 60 °C for 24 h.

2.3. Instruments

A Field Emission Gun-Scanning Electron Microscope (FEG-SEM Ultra 55 Zeiss), coupled with Energy Dispersive X-ray elemental analysis (EDX), was used to visualise the synthesized powders. In addition to these techniques, the X-ray diffraction (XRD) and TEM techniques were also used. TEM images were obtained with a JEOL 2000 FX microscope running at an accelerating voltage of 200 keV. Prior to analysis, the powders were crushed in a mortar. A small amount was then added in a small volume of pure ethanol using ultrasonic bath. A drop of this mixture was placed on a copper grid covered with a carbon coating and allowed to dry in air before analysis.

A Jobin-Yvon (LABRAM model) Raman spectrometer was used with a He–Ne laser (wavelength 632.81 nm). The 180° scattered Raman beam with respect to the incident beam was focused on the spectrometer slit. The device using a Notch filter presents a very high sensitivity which allows using weak laser intensity as low as 0.01 mW, avoiding therefore any perturbation of the polymer powder.

Doping level of polypyrrole powder was determined from the measure of the sulphur to nitrogen ratio that was carried out with the help of X-Ray Photoelectron Spectroscopy (XPS).

Conductivity of PPy powder was measured using impedance spectroscopy as well as a home made device allowing a PPy powder based disk to be pressed between the flat faces of two steel cylinders connected to a Bio-Logic SP300 potentiostat. The high frequency limit of the obtained impedance spectroscopy spectrum provides a measurement of the electronic resistance from which one can extract σ, the electronic conductivity (in $S.cm^{-1}$) of the PPy

powder by using the formula $\sigma = 1/R.l/s$, where R is the measured series resistance (in ohms), l, the thickness of the PPy powder based disk (in cm) and s, its surface (in cm^2).

2.4. Study of the polymerization of pyrrole in presence of MnO_2

The study of pyrrole polymerization reaction was realized by using optical measurements. In a preliminary series of experiments, UV-Visible spectra were recorded in the range of 350-900 nm using a Hitachi U-4001 spectrophotometer in solutions containing different concentrations of Mn^{2+} in the presence of Calix-S_4 and prepared in NaOH aqueous medium at pH 11.8, in a 1 cm standard cell. The purpose of this was to carry out a calibration procedure aimed at allowing the identification of Mn^{2+} cations in solution. It is well known that this binding agent gives a red coloration upon complexation of Mn^{2+} cations [45,46]. In order to corroborate this quantitative analysis, the presence of Mn^{2+} was also detected by cyclic voltammetry. Electrochemical measurements were carried out with a potentiostat (Gamry, Femstat FAS1). The electrochemical experiments were carried out in a usual cell containing three electrodes: a platinum electrode (area = 3.1 mm^2) as working electrode, a SCE reference electrode, and a large platinum grid as counter electrode.

3. Results and Discussion

3.1. Characterization of MnO_2 powder

The morphology of MnO_2 powder obtained from the synthesis procedure reported in section 2.2, observed by FEG-SEM is presented in Figure 1a-b. The panoramic morphology of MnO_2 powder synthesized by hydrothermal method reveals a sea urchin like morphology with 4 ~ 10 μm in diameter. Elemental analysis by EDX (Figure 1c) confirms the presence of manganese and oxygen, elemental components of MnO_2. Indeed, the presence of manganese is shown by two energy peaks appearing approximately at 5.5, and 6.3 keV whereas that of

oxygen is shown by one energy peak situated approximately at 0.3 keV. The presence of sulphur, observed as an impurity coming from manganese sulphate, is negligible.

Typical TEM image (Figure 1d) of MnO_2 powder after grinding show that the nanosticks observed previously by the FEG-SEM technique do consist of assemblies of straight sticks with diameters within the 10-50 nm range, and up to several hundreds of nanometres in length. In parallel, electron diffraction pattern showed that each stick is rather well crystallized but its orientation changes from one to another. The observed sea urchin like structure is thus a polycrystalline structure.

X-ray diffraction (XRD) pattern of the synthesized MnO_2 powder is shown in Figure 1e. The feature peaks recorded in the XRD spectrum were assigned by (hkl) values of 120, 031, 131, 230, 300, 002, 160, 401, 421, 003, 062 and 450. All of the reflections of the XRD pattern can be readily indexed to the crystallographic variety γ-MnO_2, which agrees with the values recorded in the literature (JCPDS Card. N° 14-0644).

3.2. Characterization of synthesized polypyrrole powders

The morphology of the resulting polypyrrole powder was observed by FEG-SEM (see Figs. 2a-b) and their corresponding EDX profile is presented in Figure 2c. The low magnification FEG-SEM image of polypyrrole powder synthesized from γ-MnO_2 illustrate that the synthesized polypyrrole particles exhibit hollow sea urchin like morphologies dictated by those observed for MnO_2 powder with a rather uniform size and a more or less widely open mouth. The high magnification FEG-SEM image of polypyrrole particles reveal that they are composed of many nanometric nanotubes combined together on their surface (see Figure 2b). Elemental analysis by EDX (Figure 2c) confirms the presence of carbon and nitrogen, elemental components of polypyrrole, in the structure of synthesized powders, shown by

energy peaks observed at 0.3 keV and 0.4 keV, respectively. The presence of sulphur and oxygen is also obvious in these polypyrrole powders, which suggests, at this stage, that the obtained polypyrrole powder is likely doped by SO_4^{2-} anions present in the synthesis solution, and as a consequence, that polypyrrole is in a doped, i.e. conducting state. It is worth noting the complete absence of manganese in the polypyrrole powder in spite of the use of manganese dioxide as an oxidizing agent towards pyrrole. From these first observations, it can be concluded that hollow particles of pure nanostructured polypyrrole were successfully synthesized by a chemical route.

The polypyrrole particles observed in Figs. 2b are in fact nanotubes according to TEM images. Typical TEM images (see Figure 2d) show that the nanotubes of polypyrrole powder synthesized with γ-MnO_2 observed by the FEG-SEM technique actually possess a typical outer diameter of 50 nm, a length up to 400 nm, and an inner diameter of about 10 nm which vary along the nanotube. One can also distinguish, especially from Figure 2d that those nanotubes are also closed at one extremity.

Figure 3 shows X-ray powder diffraction (XRD) pattern of the polypyrrole powder. As the absence of manganese dioxide material has been established in this material, the XRD pattern can be attributed only to polypyrrole. On Figure 3, XRD pattern exhibits a weak and broad diffraction peak at $2\theta = 25°$, which has already been encountered in literature and attributed to amorphous PPy structures [47-51].

Figure 4 presents the Raman spectrum corresponding to polypyrrole powder synthesized by using γ-MnO_2. The most important peak is the one at ca. 1599 cm^{-1}, which represents the backbone stretching mode of C=C bonds and is considered to be an overlap of the contribution of the reduced and oxidized forms of polypyrrole [52-57]. The peak positions of C=C backbone stretching bonds are in favour of dominating oxidized species. It was reported

by J. Duchet *et al.* [53] that the peak at 1503 cm^{-1} represents a skeletal band. Moreover, a broad feature comprised of several overlapping bands and centered at 1348 cm^{-1} is assigned to a hybrid mode of intra-ring C-C bond stretching and mainly inter-ring C-C bond stretching [52], antisymmetrical C-N stretching [53] or ring stretching [55,56]. The peak at 1258 cm^{-1} has been assigned to the antisymmetrical C-H in-plane bending mode [53] or N-H in-plane deformation [55]. Further evidence for the presence of oxidized species is given by the double peaks which appear at ca. 1084 cm^{-1} and 1049 cm^{-1} and assigned to the symmetrical C-H in plane bending mode associated with the bipolarons (dication) and polaron (radical cation) structures respectively [52,53]. Moreover, the bands at ca. 983 cm^{-1} and 941 cm^{-1} which are assigned to the ring deformation associated with polarons and bipolarons respectively [52,53,56] are also the signature of oxidized PPy. All these interpretations tend to demonstrate that the PPy powder is in its doped (oxidized) state, in good agreement with the presence of sulphate anions revealed by our EDX analysis.

3.3. Study of the polymerization mechanism of pyrrole

3.3.1. Optical measurements

As reported previously, MnO_2 powder, used as oxidizing agent for the chemical polymerization of pyrrole, totally disappears as such at the end of the synthesis step, as shown by the absence of manganese in the structure of the polypyrrole powders revealed by EDX and XRD. This means that manganese produced from MnO_2 reduction should be found in the supernatant solution as an ionic and therefore soluble species. These results incited us to identify the reduction product of manganese dioxide and to study the kinetics of polypyrrole polymerization reaction. In this purpose, we have used UV-Visible spectroscopy and cyclic voltammetry. In order to define the nature of these ions (Mn^{2+}, Mn^{3+}), it was postulated that

MnO_2 was reduced into Mn^{2+} ions and these ions were analyzed by the method already used by Nishida *et al.* [45].

In order to optimize the complexation conditions, Mn^{2+} aqueous solutions were prepared from different concentrations of $MnSO_4$, H_2O. The influence of Mn^{2+} concentration on the intensity of absorbance band was studied directly after mixing 1 mL of Calix-S_4 solution and 3 mL of Mn^{2+} solution, at different concentrations, at pH 11.8. It is obvious that the concentration of the testing solution affects the intensity of the absorbance band of the complex. The higher the concentration of manganese (II) cations is, the higher is the band intensity of complex Calix-S_4 / Mn (II), as presented in Figure 5, but this increase is limited at an absorbance of 3.5 because above this absorbance value, marked fluctuations appeared. The plot of this variation of absorbance with Mn^{2+} concentration shows that the absorbance of these solutions varies linearly as a function of Mn^{2+} ions concentrations, which obeys the Lambert-Beer Law (curve not shown) and constitutes thus a calibration curve.

In order to verify our hypothesis, polypyrrole powders were prepared as explained in section 2.2. After polymerization and filtration, the retrieved solution was diluted at an adequate concentration ($1.16\ 10^{-4}$ M), taking as a hypothesis that the whole initial amount of MnO_2 was reduced to Mn^{2+}. It was observed that the added volume of Calix-S_4 (1 mL) to 3 mL of retrieved diluted polymerization solution changed immediately the coloration of initial solution from colourless to red. Also, the spectrum related to the characterization of this mixture by UV-Vis, shown in Figure 6, illustrates the presence of an absorption band perfectly overlapped with that presented in Figure 5c and relative to Mn^{2+} ions at a concentration of $1.16\ 10^{-4}$ M.

In another series of experiments, the above-mentioned spectrophotometric procedure was used to follow the production of Mn^{2+} in the course of the polymerization procedure, and

therefore the reaction kinetics of the production of our polypyrrole powders. For that purpose, an adequate volume of the reaction mixture was extracted, filtered so as to remove the polypyrrole and manganese dioxide powders, and then the Mn^{2+} concentration was determined and plotted as a function of time (Figure not shown). It was found that this latter is constant with time beyond a 25 minutes reaction time, which therefore provides a first estimation of the reaction duration.

3.3.2. Electrochemical measurements

Another method allowing the identification of the reaction product resulting from MnO_2 reduction is the cyclic voltammetry technique. The aqueous solution resulting from filtration of the reaction medium was used as an electrolytic solution. The potential scan rate was 10 $mV.s^{-1}$ and the potential scan started from 0.7 V vs. SCE towards the positive direction up to 1.3 V vs. SCE, followed by a cathodic scan down to 0.7 V vs. SCE. The resulting cyclic voltammogram shown on Figure 7 is typical for the electrochemical behaviour of Mn^{2+} cations in acidic aqueous solutions. The reaction product was therefore undoubtedly identified as Mn^{2+}. The anodic peak indeed reveals the oxidation of dissolved Mn^{2+} cations into manganese dioxide, produced as an insoluble thin film on the working electrode surface, whereas the cathodic peak reveals its reduction in the reverse reaction [58]. This important observation demonstrates that the Mn^{2+} ions that were not detected in the structure of the produced polypyrrole powders are present in the retrieved polymerization solution of pyrrole and consequently confirms the results obtained by the UV-Visible technique.

3.4 Discussion

From these results, it can be concluded that the manganese dioxide sea urchins have oxidized pyrrole to produce hollow sea urchin shaped polypyrrole particles (see Eq. 1 with the hypothesis that the doping rate in PPy is 0.33 per monomer [59]) and were reduced into Mn^{2+} cations (see Eq. 2), which were produced in solution as soluble species.

$$nPy \rightarrow (Py^{0.33+})_n + 2nH^+ + 2.33ne^- \qquad \text{(Eq. 1)}$$

$$MnO_2 + 4H^+ + 2e^- \rightarrow Mn^{2+} + 2H_2O \qquad \text{(Eq. 2)}$$

This redox mechanism can be represented by the following redox reaction:

$$7nMnO_2 + 16nH^+ + 6nPy \rightarrow 7nMn^{2+} + 14nH_2O + 6(Py^{0.33+})_n \qquad \text{(Eq.3)}$$

In our experiments, oxidation of pyrrole occurred at the manganese dioxide/aqueous solution interface, leading to the progressive dissolution of MnO_2 into soluble Mn^{2+} cations. As this interface therefore steps back towards the heart of the initial MnO_2 particles, the polypyrrole particles are likely to grow towards the interior of the native particles, so as to keep in touch with the manganese dioxide surface, although this is not incompatible with a simultaneous growth on the external side of the growing PPy particles. Such mechanism may suggest that pyrrole monomers and sulphate anions may diffuse through the growing and hollow polypyrrole particles envelope from the outside to the inside so as to feed the reaction site with reactants. Simultaneously, Mn^{2+} cations have to diffuse away through the walls of these polypyrrole structures so as to leave the reaction site where they were produced. Another possibility, possibly more realistic, is that reactants and reaction products respectively reach and leave the reaction site by using the mouth frequently observed on the resulting hollow sea urchin shaped polypyrrole particles. In any case, it is obvious from our structural characterization experiments that these manganese dioxide nanostructured particles did not act only as oxidizing agents in the course of this mechanism but also as sacrificial templates

imposing their shape to the resulting polypyrrole particles during a so-called core-shell redox mechanism.

The resulting polypyrrole powder possesses a 0.31 doping level as shown by XPS characterisation (see Survey XPS spectrum in Figure SI 1 of Supplementary Information). Such value is in very good agreement with that of 0.33 usually encountered in literature for polypyrrole [59]. Moreover impedance spectroscopy measurements allowed us to determine a series resistance of 282.4 ± 4.4 Ω (average value calculated over ten impedance spectroscopy measurements, see impedance spectroscopy spectrum in Figure SI 2 of Supplementary Information) and thus a 0.05 $S.cm^{-1}$ conductivity. By comparison with the doping level value, this conductivity value may reveal conductivity limitations due to chain length and nanostructured character of polypyrrole powders. The nanotubes observed on the surface of the sea-urchin shaped polypyrrole nanostructures are about two hundred fifty nanometers long and their walls are about twenty-five nanometers thick (see Figure 2). As a consequence, one can expect a majority of short polypyrrole chain lengths that is likely to lead to a higher number of interchain electron transfer events and therefore to a lower conductivity, especially in an amorphous material (see Figure 3) like the polypyrrole powder synthesised in this work.

Conclusion

In this contribution, hollow sea-urchin shaped nanostructured polypyrrole particles were successfully synthesised by using sea urchin shaped MnO_2 nanostructured powders as oxidizing agents and sacrificial templates simultaneously. The reaction kinetics of pyrrole polymerization was studied by UV-Visible spectroscopy and cyclic voltammetry measurements. The reaction was found to occur within about 25 minutes. We demonstrated that MnO_2 particles oxidize pyrrole monomers into oxidised polypyrrole and were reduced to

soluble Mn^{2+} cations identified in the retrieved polymerization solution, which explains the absence of manganese in the produced polypyrrole powders. The reaction mechanism is clearly redox and of the core-shell type. The synthesized amorphous polypyrrole powders were found to be doped with sulphate anions and thus in the conducting state. They possess a 0.31 doping level as well as a 0.05 $S.cm^{-1}$ conductivity in our experimental conditions. From all these observations, it can be mentioned that we have accurately and undoubtedly defined an easy and direct method to synthesize large amounts of pure, amorphous, conducting and nanostructured polypyrrole particles that are likely to possess in addition a high specific area.

We also believe that our investigations bring a necessary light on the redox reactivity between MnO_2 and pyrrole monomer that was rather badly defined in literature so far. As such, they may affect strongly and beyond expectations i) the understanding of chemical synthesis of PPy in the presence of MnO_2 and another oxidizing agent, ii) the electrochemical deposition of composite polypyrrole/MnO_2 thin films, and iii) the expectable surface properties (oxidation power) of MnO_2 particles in the resulting materials, keeping in mind that the oxidation potential of polypyrrole is lower than the oxidation potential of pyrrole. It is likely that such conclusions will be of large interest for numerous investigations frequently reported in literature lately concerning the synthesis, properties and applications of PPy/MnO_2 powders (mixtures or core/shell) and PPy/MnO_2 composite thin films in view of applications as electrode materials in batteries, supercapacitors and electrocatalysis for instance.

Acknowledgements

The present work was carried out in the frame of French – Algerian cooperation project CMEP- PHC Tassili N°06 MDU 686. The authors are grateful to EGIDE for financial support. They thank Mrs Pillier and Mr. Borensztajn for their efficient assistance in TEM,

FEG-SEM and EDX experiments, as well as Mr C. Bazin and Mrs. H. Benidiri for the XRD measurements. Mr C. Calers (LRS, UMR 7197) is warmly acknowledged for his collaboration during XPS measurements.

REFERENCES

[1] V.H. Grassian, When size really matters: Size-dependent properties and surface chemistry of metal and metal oxide nanoparticules in gas and liquid phase environments, J. Phys. Chem. C 112 (2008) 18303-18313.

[2] L. Hu, D.S. Hecht and G. Grüner, Carbon nanotube thin films: fabrication, properties, and applications, Chem. Rev. 110 (2010) 5790-5844.

[3] G.R. Patzke, Y. Zhou, R. Kontic and F. Conrad, Oxide nanomaterials: Synthetic developments, mechanistic studies and technological innovations, Angew. Chem., Int. Ed. 50 (2010) 2.

[4] L. Benhaddad, L. Makhloufi, B. Messaoudi, K. Rahmouni and H. Takenouti, Reactivity of nanostructured MnO_2 in alkaline medium studied with a microcavity electrode: Effect of synthesizing agent, J. Mater. Sci. Technol. 27 (2011) 585-593.

[5] L. Benhaddad, L. Makhloufi, B. Messaoudi, K. Rahmouni and H. Takenouti, Reactivity of nanostructured MnO2 in alkaline medium studied with a micro-cavity electrode: Effect of synthesizing temperature, ACS Appl. Mater. Interfaces 1 (2009) 424-432.

[6] Y.-Z. Long, M.-M. Li, C. Gu, M. Wanc, J.-L. Duvail, Z. Liu, Z. Fan, Recent advances in synthesis, physical properties and applications of conducting polymer nanotubes and nanofibers, Prog. Polym. Sci. 36 (2011) 1415-1442.

[7] J. Jang, Conducting polymer nanomaterials and their applications (Review), Adv. Polym. Sci. 199 (2006) 189-259.

[8] N.T.L. Hien, B. Garcia, A. Pailleret and C. Deslouis, Role of doping ions in the corrosion protection of iron by polypyrrole films, Electrochim. Acta 50 (2005) 1747-1755.

[9] A. Pailleret, N.T.L. Hien, D.T.M. Thanh and C. Deslouis, Surface reactivity of polypyrrole/iron-oxide nanoparticles: electrochemical and CS-AFM investigations, J. Solid State Electrochem. 11 (2007) 1013-1021.

[10] C.A. Vetter, A. Suryawanshi, J.R. Lamb, B. Law and V.J. Gelling, Novel synthesis of stable polypyrrole nanospheres using ozone, Langmuir 27 (2011) 13719-13728.

[11] Z.P. Zhang, F. Wang, F.E. Chen and G.Q. Shi, Preparation of polythiophene coated gold nanoparticles, Mater. Lett. 60 (8) (2006) 1039-1042.

[12] J.X. Huang and R.B. Kaner, Nanofiber formation in the chemical polymerization of aniline: A mechanistic study, Angew. Chem., Int. Ed., 43 (2004) 5817-5821.

[13] K. Huang, M.X. Wan, Y. Long, Z. Chen and Y. Wei, Multi-functional polypyrrole nanofibres via a functional dopant-introduced process, Synth. Met. 155 (2005) 495-500.

[14] L. Liu, C. Zhao, Y. Zhao, N. Jia, Q. Zhou, M. Yan and Z. Jiang, Characteristics of polypyrrole (PPy) nano-tubules made by templated ac-electropolymerization, Eur. Polym. J. 41 (2005) 2117-2121.

[15] C. Debiemme-Chouvy, Template-free one-step electrochemical formation of polypyrrole nanowire array, Electrochem. Commun. 11 (2009) 298-301.

[16] G. Lu, C. Li and G. Shi, Polypyrrole micro- and nanowires synthesized by electrochemical polymerization of pyrrole in the aqueous solutions of pyrenesulfonic acid, Polymer 47 (2006) 1778-1784.

[17] C. Jérôme, D.E. Labaye and R. Jérôme, Electrochemical formation of polypyrrole nanowires, Synth. Met. 142 (2004) 207-216.

[18] D. Voss, Cheap and cheerful circuits, Nature 407 (2000) 442-444.

[19] J. Janata and M. Josowicz, Conducting polymers in electronic chemical sensors, Nature Mater. 2 (2003) 19-24.

[20] A.A. Argun, A. Cirpan and J.R. Reynolds, The first truly all-polymer electrochromic devices, Adv. Mater. 15 (2003) 1338-1341.

[21] S. Mokrane, L. Makhloufi, H. Hammache and B. Saidani, Electropolymerization of polypyrrole, modified with germanium, on a passivated titanium electrode in aqueous nitrate solution: new results on catalytic reduction of protons and dissolved oxygen, J. Solid State Electrochem. 5 (2001) 339-347.

[22] D. Oukil, L. Makhloufi and B. Saidani, Preparation of polypyrrole films containing ferrocyanide ions deposited onto thermally pre-treated and untreated iron substrate: Application in the electroanalytical determination of ascorbic acid, Sens. Actuators, B 123 (2) (2007) 1083-1089.

[23] M.B. González, S.B. Saidman, Electrosynthesis of hollow polypyrrole microtubes with a rectangular cross-section, Electrochem. Commun. 13 (2011) 513-516.

[24] A.H. Chen, H.Q. Wang, B. Zhao and X.Y. Li, Preparation of polypyrrole-Fe_3O_4 nanocomposites by the use of common ion effect, Synth. Met. 139 (2003) 411-415.

[25] M. Wei and Y. Lu, Templating fabrication of polypyrrole nanorods/nanofibers, Synth. Met. 159 (2009) 1061-1066.

[26] J.M. Mativetsky and W.R. Datars, Morphology and electrical properties of template-synthesized polypyrrole nanocylinders, Physica B, 324 (2002) 191-204.

[27] G. Cao and D. Liu, Template-based synthesis of nanorod, nanowire, and nanotube arrays, Adv. Colloid and Interface Sci. 136 (2008) 45-64.

[28] L. Dauginet-Da Pra and S. Demoustier-Champagne, Investigation of the electronic structure and spectroelectrochemical properties of conductive polymer nanotubes arrays, Polymer 46 (2005) 1583-1594.

[29] X. Zhang and S.K. Manohar, Narrow pore-diameter polypyrrole nanotubes, J. Am. Chem. Soc. 127 (2005) 14156-7.

[30] C.R. Martin, Nanomaterials - a membrane-based synthetic approach, Science 266 (1994) 1961-1966.

[31] J. Jang and H. Yoon, Facile fabrication of polypyrrole nanotubes using reverse microemulsion polymerization, Chem. Commun. (2003) 720.

[32] M.X. Wan, K. Huang and L.J. Zhang, Nanotubes of Conducting Polyaniline and Polypyrrole, Int. J. Nonlinear Sci. Numer. Simul. 3 (3-4) (2002) 465-468.

[33] N. Ballav, High-conducting polyaniline via oxidative polymerization of aniline by MnO_2, PbO_2 and NH_4VO_3, Mater. Lett. 58 (2004) 3257-3260.

[34] L. Pan, L. Pu, Y. Shi, S. Song, Z. Xu, R. Zhang, Y. Zheng, Synthesis of Polyaniline Nanotubes with a Reactive Template of Manganese Oxide, Adv. Mater. 19 (2007) 461-464.

[35] A.H. Gemeay, I.A. Mansour, R.G. El-Sharkawy and A.B. Zaki, Preparation and characterization of polyaniline/manganese dioxide composites via oxidative polymerization: Effect of acids, Eur. Polym. J. 41 (2005) 2575-2583.

[36] A.H. Gemeay, I.A. Mansour, R.G. El-Sharkawy and A.B. Zaki, Preparation and characterization of polyaniline/manganese dioxide composites and their catalytic activity, J. Colloid Interface Sci. 308 (2007) 385-394.

[37] F. Yang, Y. Chu, S. Ma, Y. Zhang and J. Liu, Preparation of uniform silica/polypyrrole core/shell microspheres and polypyrrole hollow microspheres by the template of modified

silica particles using different modified agents, J. Colloid Interface Sci. 301 (2006) 470-478.

[38] D.G. Shchukin, G.B. Sukhorukov and H. Mohwald, Smart Inorganic/Organic Nanocomposite Hollow Microcapsules, Angew. Chem., Int. Ed. 42 (2003) 4472-4479.

[39] D. Cheng, H. Xia and H.S.O. Chan, Facile fabrication of AgCl/polypyrrole-chitosan core-shell nanoparticles and polymeric hollow nanospheres, Langmuir 20 (2004) 9909-9912.

[40] H. Nguyen Thi Le, M.C. Bernard, B. Garcia-Renaud, C. Deslouis, Raman spectroscopy analysis of polypyrrole films as protective coatings on iron, Synth. Met. 140 (2004) 287-293.

[41] J.J. Hu, Y.P. Duan, J. Zhang, H. Jing, S.H. Liu and W.P. Li, gamma-MnO_2/polyaniline composites: Preparation, characterization, and applications in microwave absorption Phys. B 406 (2011) 1950-1955.

[42] Z.H. Dong, Y.L. Wei, W. Shi, G.A. Zhang, Characterisation of doped polypyrrole/manganese oxide nanocomposite for supercapacitor electrodes, Mater. Chem. Phys. 131 (2011) 529-534.

[43] A.H. Gemeay, H. Nishiyama, S. Kuwabata, H. Yoneyama, Chemical preparation of Manganese dioxide/polypyrrole composites and their use as cathode active materials for rechargeable lithium batteries, J. Electrochem. Soc. 42 (1995) 4190-4195.

[44] H. Manjunatha, G. S. Suresh and T. V. Venkatesha, Electrode materials for aqueous rechargeable lithium batteries, J. Solid State Electrochem. 45 (2011) 431-445.

[45] N. Yamamoto, M. Nishida, I. Yoshida, F. Sagara, K. Ueno, D. Ishii and S. Shinkai, Spectrophotometric determination of manganese(II) with tetrasodium 25,26,27,28-tetrahydroxycalix[4]arene-5,11,17,23-tetrasulfonate, Bunseki Kagaku 43 (1994) 45-50.

[46] S. Shinkai, S. Mori, T. Tsubaki, T. Sone and O. Manabe, new water-soluble host molecules derived from calix[6]arene, Tetrahedron Lett. 25 (46) (1984) 5315-5318.

[47] H. Zhang, X. Zhong, J.-. Xu and H.-Y. Chen, Fe_3O_4/polypyrrole/Au nanocomposites with core/shell/shell structure: synthesis, characterization and their electrochemical properties, Langmuir 24 (2008) 13748-52.

[48] J. Li, L. Cui and X. Zhang, Preparation and electrochemistry of one-dimensional nanostructured MnO_2/PPy composite for electrochemical capacitor, Appl. Surf. Sci. 256 (2010) 4339-4343.

[49] D.K. Kim, K.W. Oh, H.J. Ahn and S.H. Kim, Synthesis and characterization of polypyrrole rod doped with *p*-toluenesulfonic acid via micelle formation, J. Appl. Polym. Sci. 107 (6) (2008) 3925-3932.

[50] Z. Gu, C. Li, G. Wang, L. Zhang, X. Li, W. Wang and S. Jin, Synthesis and characterization of polypyrrole/graphite oxide composite by *in situ* emulsion polymerization, J. Polym. Sci., Part B: Polym. Phys. 48 (12) (2010) 1329-1335.

[51] C. Yang and P. Liu, Polypyrrole/conductive mica composites: Preparation, characterization, and application in supercapacitor, Synth. Met. 160 (2010) 768-773.

[52] Y. Furukawa, S. Tazawa, Y. Fujii, and I. Harada, Raman spectra of polypyrrole and its 2,5-^{13}C-substituted and C-deuterated analogues in doped and undoped states, Synth. Met. 24 (1988) 329-341.

[53] J. Duchet, R. Legras and S. Demoustier-Champagne, Chemical synthesis of polypyrrole: structure–properties relationship, Synth. Met. 98 (1998) 113-122.

[54] Y.C. Liu and B.-J. Hwang, Identification of oxidized polypyrrole on Raman spectrum, Synth. Met. 113 (2000) 203-207.

[55] Y.C. Liu, B.-J. Hwang, W.-J. Jian and R. Santhanam, In situ cyclic voltammetry-surface-enhanced Raman spectroscopy: studies on the doping–undoping of polypyrrole film, Thin Solid Films 374 (2000) 85-91.

[56] F. Chen, G. Shi, M. Fu, L. Qu and X. Hong, Raman spectroscopic evidence of thickness dependence of the doping level of electrochemically deposited polypyrrole film, Synth. Met. 132 (2003) 125.

[57] I. Harada and Y. Furukawa, in Vibrational Spectra and Structure, J.R. Durig Ed., Elsevier, Amsterdam 19 (1991) 369.

[58] R. L. Paul and A. Cartwright, The mechanism of the deposition of manganese-dioxide .2. electrode impedance studies**,** J. Electroanal. Chem. 201 (1) (1986) 113-122.

[59] A. Deronzier, J-C. Moutet, Polypyrrole films containing metal complexes: syntheses and applications, Coord. Chem. Rev. 147 (1996) 339-371.

FIGURES CAPTIONS

Figure 1: (a-b) FEG-SEM images, (c) EDX profile, (d) TEM image and (e) XRD pattern of MnO_2 powder.

Figure 2: (a) Low magnification and (**b)** high magnification FEG-SEM images, **(c)** EDX profile, and **(d)** TEM image of polypyrrole powder synthesized with γ-MnO_2.

Figure 3: XRD pattern of polypyrrole powder synthesized with γ-MnO_2.

Figure 4: Raman spectrum of polypyrrole powder synthesized with γ-MnO_2.

Figure 5: UV-Visible spectra of Calix-S_4/Mn^{2+} complex in aqueous solutions containing Calix-S_4 (1 mL) and Mn^{2+} (3 mL) at different concentrations: **(a)** 0,29 10^{-4} M, **(b)** 0,58 10^{-4} M, **(c)** 1,16 10^{-4} M, **(d)** 1,74 10^{-4} M, **(e)** 2,32 10^{-4} M, **(f)** 2,9 10^{-4} M, **(g)** 3,48 10^{-4} M, **(h)** 4,06 10^{-4} M, **(i)** 4,64 10^{-4} M, **(j)** 5,22 10^{-4} M, **(k)** 5,8 10^{-4} M.

Figure 6: Overlapped UV-Visible spectra showing **(a)** that presented in Figure 6 (c) and **(b)** that recorded in an aqueous solution containing Calix-S_4 (1 mL) and 3 mL of retrieved polymerization solution diluted so as to get the same Mn^{2+} concentration (1,16 10^{-4} M), taking as an hypothesis that the whole initial amount of MnO_2 was reduced to Mn^{2+}.

Figure 7: Cyclic voltammogramm of platinum electrode in retrieved polymerization solution diluted so as to get the same Mn^{2+} concentration (1,16 10^{-4} M), taking as an hypothesis that the whole initial amount of MnO_2 was reduced to Mn^{2+}. Potential scan rate: 10 $mV.s^{-1}$.

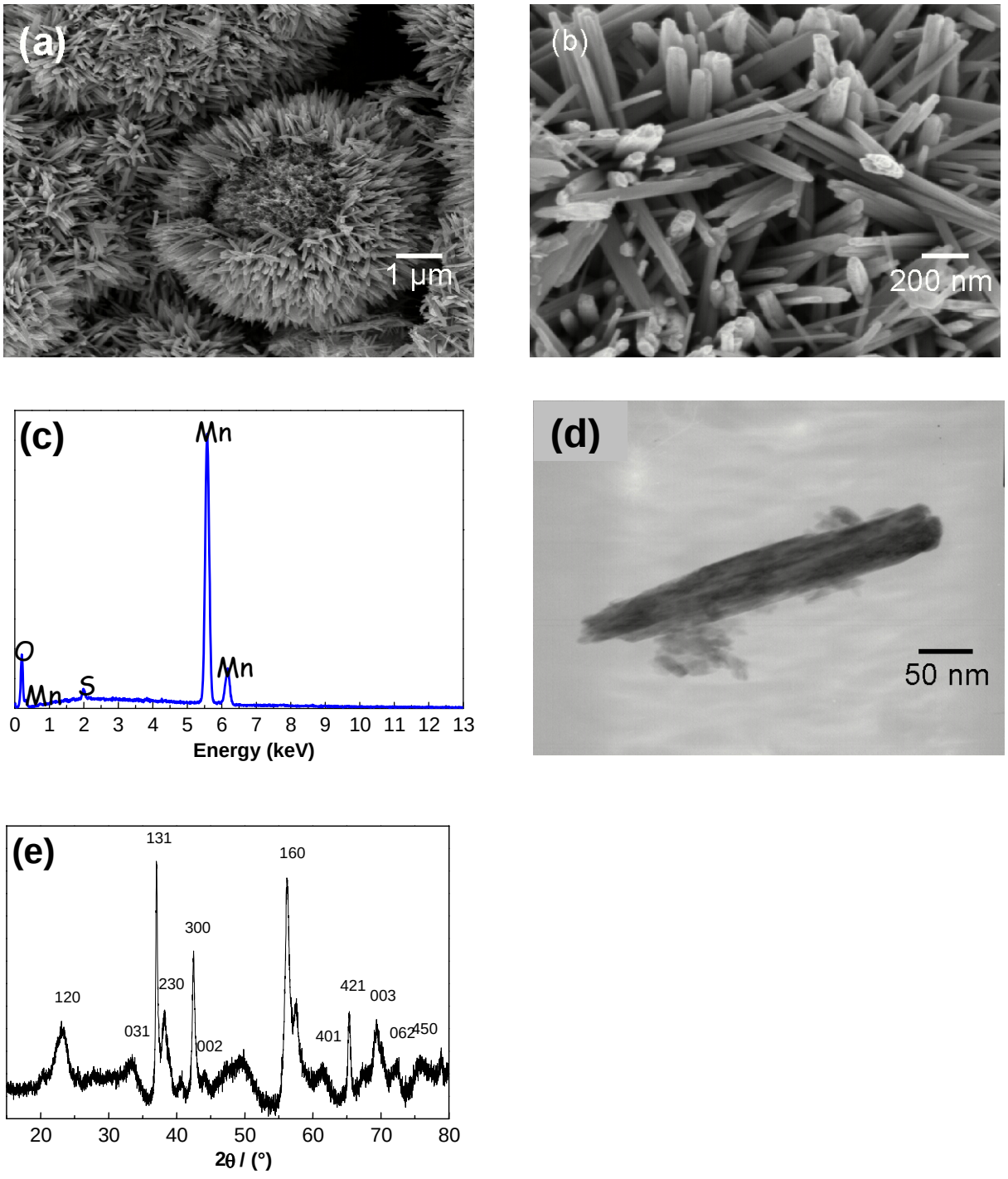

Figure 1: (a-b) FEG-SEM images, (c) EDX profile, (d) TEM image and (e) XRD pattern of MnO_2 powder.

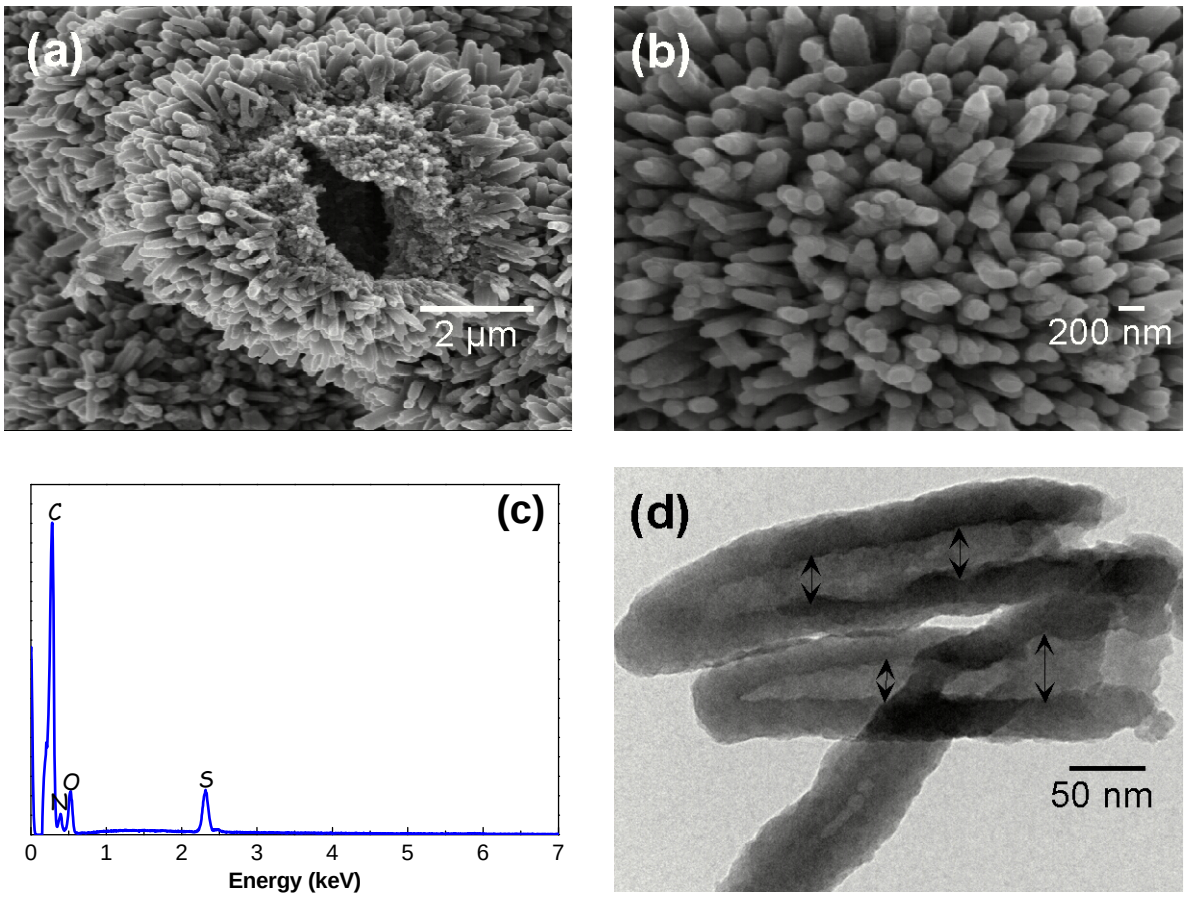

Figure 2: (a) Low magnification and (**b)** high magnification FEG-SEM images, **(c)** EDX profile, and **(d)** TEM image of polypyrrole powder synthesized with γ-MnO_2.

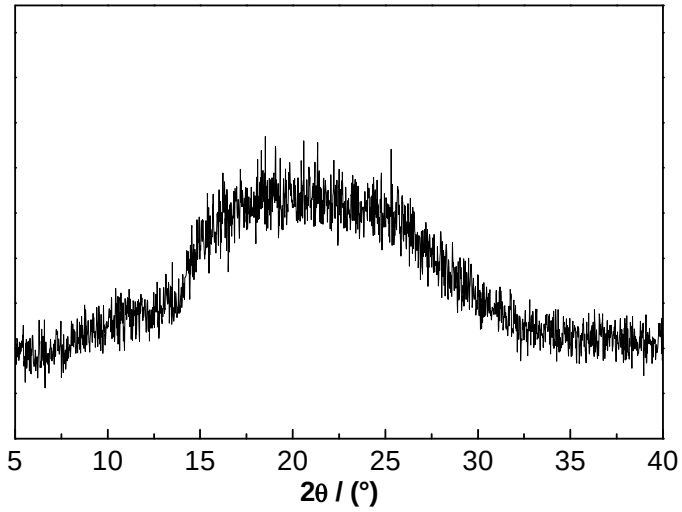

Figure 3: XRD pattern of polypyrrole powder synthesized with γ-MnO_2.

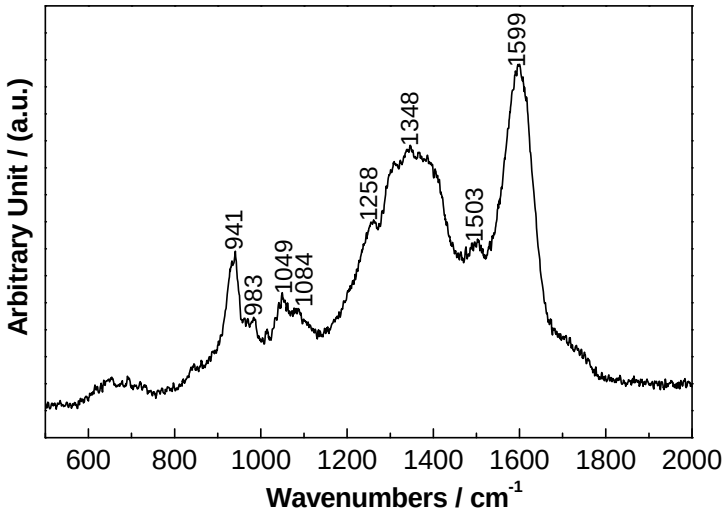

Figure 4: Raman spectrum of polypyrrole powder synthesized with γ-MnO_2.

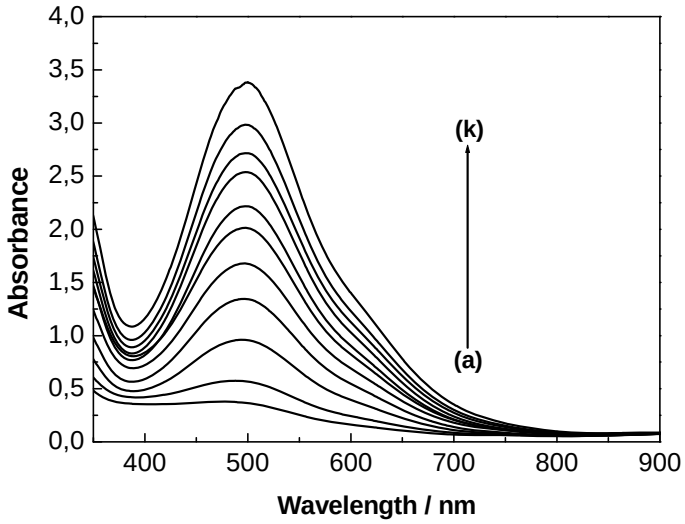

Figure 5: UV-Visible spectra of Calix-S_4/Mn^{2+} complex in aqueous solutions containing Calix-S_4 (1 mL) and Mn^{2+} (3 mL) at different concentrations: **(a)** 0,29 10^{-4} M, **(b)** 0,58 10^{-4} M, **(c)** 1,16 10^{-4} M, **(d)** 1,74 10^{-4} M, **(e)** 2,32 10^{-4} M, **(f)** 2,9 10^{-4} M, **(g)** 3,48 10^{-4} M, **(h)** 4,06 10^{-4} M, **(i)** 4,64 10^{-4} M, **(j)** 5,22 10^{-4} M, **(k)** 5,8 10^{-4} M.

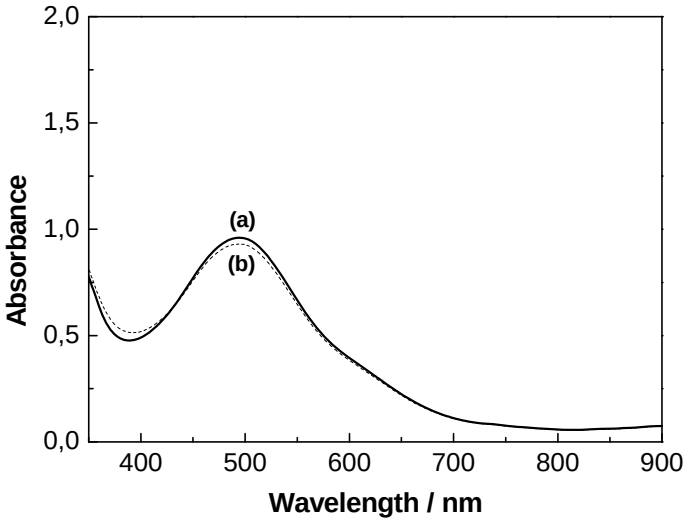

Figure 6: Overlapped UV-Visible spectra showing **(a)** that presented in Fig. 6 (c) and **(b)** that recorded in an aqueous solution containing Calix-S_4 (1 mL) and 3 mL of retrieved polymerization solution diluted so as to get the same Mn^{2+} concentration (1,16 10^{-4} M), taking as an hypothesis that the whole initial amount of MnO_2 was reduced to Mn^{2+}.

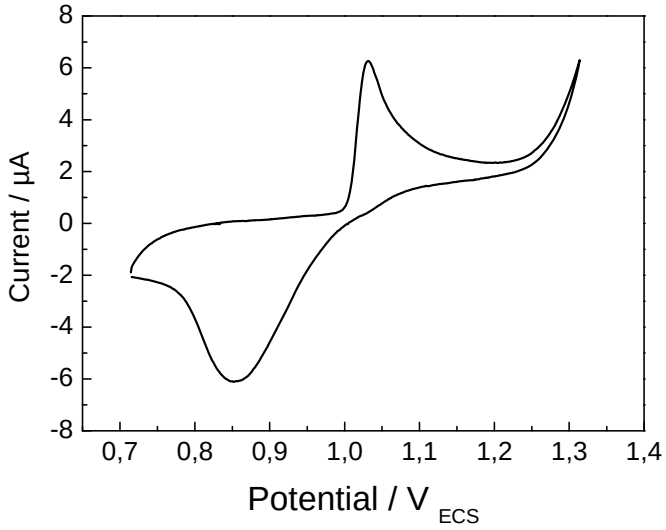

Figure 7: Cyclic voltammogramm of platinum electrode in retrieved polymerization solution diluted so as to get the same Mn^{2+} concentration (1,16 10^{-4} M), taking as an hypothesis that the whole initial amount of MnO_2 was reduced to Mn^{2+}. Potential scan rate: 10 $mV.s^{-1}$.